Inorg. Chem. **2009**, *48*, 2436−2442

Three-Dimensional Metal-Organic Frameworks Based on Functionalized Tetracarboxylate Linkers: Synthesis, Strucures, and Gas Sorption Studies

Shuting Wu,[†,‡] Liqing Ma,[†] La-Sheng Long,[‡] Lan-Sun Zheng,[‡] and Wenbin Lin*[,†]

Department of Chemistry, University of North Carolina at Chapel Hill, Chapel Hill, North Carolina 27599, and State Key Laboratory for Physical Chemistry of Solid Surfaces, Department of Chemistry, Xiamen University, Xiamen, Fujian 361005, China

Received August 27, 2008

New tetracarboxylate ligands with dihydroxy ($\mathbf{L_1}$) and crown ether functionalities ($\mathbf{L_2}$) have been synthesized and treated with Cu^{II} and Zn^{II} ions to generate three-dimensional (3D) metal-organic frameworks (MOFs) with the compositions of $[Cu_2(\mathbf{L_1})(H_2O)_2]\cdot 14DMF\cdot 10H_2O$, **5**, $[Cu_2(\mathbf{L_2})(H_2O)_2]\cdot 12DMF$, **6**, $[Zn_6(\mu_4\text{-}O)(\mathbf{L_1})_2(\mathbf{L_1}\text{-}H_2)]\cdot 35DMF\cdot 27H_2O$, **7**, and $[Zn_3Na_2(\mathbf{L_2})_2(DMF)_2]\cdot 7DMF\cdot 14H_2O$, **8**. The four compounds show different framework structures with different connectivities. Compound **5** exhibits the PtS topology whereas compound **6** has a $[6^4.8^2]_3[6^6]$ topology. Compound **7** adopts a new $[4.6^5][4^2.6^8][4^4.6^2][4^5.6][4^8.6^{10}.8^3]$ topology while compound **8** exhibits the Flu topology. The porosity and H_2 uptake were studied by gas sorption experiments and grand canonical Monte Carlo (GCMC) simulations. Compound **5** shows a high H_2 uptake of up to 1.11 wt % at 77 K.

Introduction

Metal-organic frameworks (MOFs) have attracted a great deal of recent interest because of their potential applications in a number of areas, including hydrogen storage,[1−8] heterogeneous catalysis,[9−13] nonlinear optics,[14,15] and host−guest induced separation.[16,17] To fully realize their potential, reliable synthetic strategies are needed for incorporating exploitable functionalities into these MOFs. We have developed several complimentary strategies to prepare functional MOFs, including post-synthetic modifications of homochiral MOFs for heterogeneous asymmetric catalysis,[13,18] direct incorporation of catalytically active metal centers into MOFs,[19−21] and delivery of anticancer cisplatin prodrugs in an amorphous nanoscale MOF.[22]

Among many organic bridging ligands, those of multiple carboxylate groups have emerged as ideal linkers for building

* To whom correspondence should be addressed. E-mail: wlin@unc.edu.
† University of North Carolina at Chapel Hill.
‡ Xiamen University.

(1) Rosi, N. L.; Eckert, J.; Eddaoudi, M.; Vodak, D. T.; Kim, J.; O'Keeffe, M.; Yaghi, O. M. *Science* **2003**, *300*, 1127–1129.
(2) Kitagawa, S.; Kitaura, R.; Noro, S. *Angew. Chem., Int. Ed.* **2004**, *43*, 2334–2375.
(3) Chen, B. L.; Ockwig, N. W.; Millward, A. R.; Contreras, D. S.; Yaghi, O. M. *Angew. Chem., Int. Ed.* **2005**, *44*, 4745–4749.
(4) Dincă, M.; Long, J. R. *J. Am. Chem. Soc.* **2005**, *127*, 9376–9377.
(5) Kesanli, B.; Cui, Y.; Smith, M. R.; Bittner, E. W.; Bockrath, B. C.; Lin, W. B. *Angew. Chem., Int. Ed.* **2005**, *44*, 72–75.
(6) Matsuda, R.; Kitaura, R.; Kitagawa, S.; Kubota, Y.; Belosludov, R. V.; Kobayashi, T. C.; Sakamoto, H.; Chiba, T.; Takata, M.; Kawazoe, Y.; Mita, Y. *Nature* **2005**, *436*, 238–241.
(7) Latroche, M.; Surblé, S.; Serre, C.; Mellot-Draznieks, C.; Llewellyn, P. L.; Lee, J. H.; Chang, J. S.; Jhung, S. H.; Férey, G. *Angew. Chem., Int. Ed.* **2006**, *45*, 8227–8231.
(8) Mircea, D.; Long, J. R. *Angew. Chem., Int. Ed.* **2008**, *47*, 6766–6779.
(9) Wu, C. D.; Lin, W. B. *Angew. Chem., Int. Ed.* **2005**, *44*, 1958–1961.
(10) Dybtsev, D. N.; Nuzhdin, A. L.; Chun, H.; Bryliakov, K. P.; Talsi, E. P.; Fedin, V. P.; Kim, K. *Angew. Chem., Int. Ed.* **2006**, *45*, 916–920.
(11) Mueller, U.; Schubert, M.; Teich, F.; Puetter, H.; Schierle-Arndt, K.; Pastré, J. *J. Mater. Chem.* **2006**, *16*, 626–636.
(12) Zou, R. Q.; Sakurai, H.; Xu, Q. *Angew. Chem., Int. Ed.* **2006**, *45*, 2542–2546.
(13) Wu, C. D.; Lin, W. B. *Angew. Chem., Int. Ed.* **2007**, *46*, 1075–1078.
(14) Lin, W. B.; Wang, Z. Y.; Ma, L. *J. Am. Chem. Soc.* **1999**, *121*, 11249–11250.
(15) Evans, O. R.; Lin, W. B. *Acc. Chem. Res.* **2002**, *35*, 511–522.
(16) Fletcher, A. J.; Cussen, E. J.; Bradshaw, D.; Rosseinsky, M. J.; Thomas, K. M. *J. Am. Chem. Soc.* **2004**, *126*, 9750–9759.
(17) Alaerts, L.; Kirschhock, C. E. A.; Maes, M.; van der Veen, M. A.; Finsy, V.; Depla, A.; Martens, J. A.; Baron, G. V.; Jacobs, P. A.; Denayer, J. E. M.; De Vos, D. E. *Angew. Chem., Int. Ed.* **2007**, *46*, 4293–4297.
(18) Wu, C.-D.; Hu, A.; Zhang, L.; Lin, W. *J. Am. Chem. Soc.* **2005**, *127*, 8940–8941.
(19) Evans, O. R.; Ngo, H. L.; Lin, W. *J. Am. Chem. Soc.* **2001**, *123*, 10395–10396.
(20) Hu, A.; Ngo, H. L.; Lin, W. *J. Am. Chem. Soc.* **2003**, *125*, 11490–11491.
(21) Hu, A.; Ngo, H. L.; Lin, W. *Angew. Chem., Int. Ed.* **2003**, *42*, 6000–6003.
(22) Rieter, W. J.; Pott, K. M.; Taylor, K. M. L.; Lin, W. *J. Am. Chem. Soc.* **2008**, *130*, 11584–11585.

10.1021/ic801631w CCC: $40.75
Published on Web 02/18/2009

Chart 1

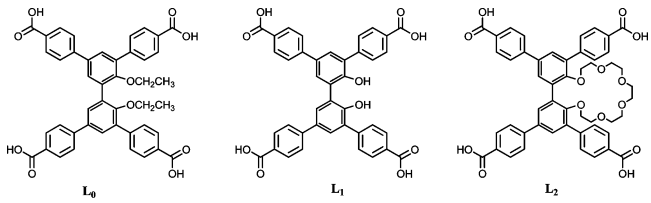

MOFs.[23] For example, elongated dicarboxylate ligands have been used to construct a family of porous IRMOFs,[1,24] whereas tricarboxylate ligands have been used by several groups to construct mesoporous MOFs.[25−27] Schröder and co-workers have used coplanar tetracarboxylate ligands to construct porous MOFs that exhibit significant hydrogen uptake.[28] We recently reported the synthesis of isostructural Cu and Zn MOFs using an elongated tetracarboxylate linker ($\mathbf{L_0}$ as shown in Chart 1) based on the biphenol system.[29] Unlike previously reported linkers, our ligand system contains dialkoxy groups that can be deprotected under appropriate conditions to reveal the dihydroxy functional group (see $\mathbf{L_1}$). The dihydroxy group in $\mathbf{L_1}$ can be further derivatized to lead to a tetracarboxylate linker with a crown ether moiety (see $\mathbf{L_2}$). The biphenol-derived tetracarboxylate ligand is thus highly tailorable and provides an interesting system for examining the dependence of MOF structures and topologies on ligand modifications. Herein we report the synthesis and structures of four Cu and Zn MOFs based on new biphenol-derived tetracarboxylate ligands containing dihydroxy and crown ether functionalities. Network topologies and gas sorption capacities of these three-dimensional (3D) MOFs are also examined.

Results and Discussion

Synthesis. Treatment of previously synthesized 2,2′-diethoxylbiphenyl-3,3′,5,5′-tetrakis(4-methylbenzoate) (**1**)[29] with BBr_3 followed by aqueous workup led to complete deprotection of both the ethoxy and the methyl ester groups and afforded $\mathbf{L_1}$-H_4 in 98.5% yield. To functionalize the biphenol tetracarboxylate ligand with a crown ether moiety, the intermediate 3,3′,5,5′-tetrabromo-2,2′-penta(ethylene glycol)biphenyl (**3**) was prepared by treating 3,3′,5,5′-tetrabromo-2,2′-biphenol (**2**) with penta(ethylene glycol) di-*p*-toluenesulfonate and NaH in anhydrous tetrahydrofuran (THF).[30,31] 2,2′-Penta(ethylene glycol)biphenyl-3,3′,5,5′-tetrakis(4-methylbenzoate) (**4**) was prepared by Pd-catalyzed Suzuki coupling between **3** and 4-(methoxycarbonyl)phenylboronic acid in 75.8% yield. Tetracarboxylic acid $\mathbf{L_2}$-H_4 was prepared by base-catalyzed hydrolysis of **4**. All of the intermediates (**1**−**4**) and $\mathbf{L_1}$-H_4 and $\mathbf{L_2}$-H_4 were characterized by ^{1}H NMR spectroscopy. Single crystals of $[Cu_2(\mathbf{L_1})(H_2O)_2]\cdot 14DMF\cdot 10H_2O$ (**5**), $[Zn_6(\mu_4\text{-}O)(\mathbf{L_1})_2(\mathbf{L_1}\text{-}H_2)]\cdot 35DMF\cdot 27H_2O$ (**7**), or $[Zn_3Na_2(\mathbf{L_2})_2(DMF)_2]\cdot 7DMF\cdot 14H_2O$ (**8**) were obtained when $\mathbf{L_1}$-H_4 or $\mathbf{L_2}$-H_4 was treated with Cu^{II} or Zn^{II} salts in DMF/H_2O solution at 60 °C (DMF, *N*,*N*-dimethylformamide). Single crystals of $[Cu_2(\mathbf{L_2})(H_2O)_2]\cdot 12DMF$ (**6**) were obtained after crystallization in DMF/H_2O solution at 80 °C. For compounds **6** and **8**, addition of Na^+ and K^+ salts improved the quality of single crystals. The Na^+ ions coordinate to the crown ether groups in **8** and therefore reduce the disorder of the crown ether group. The alkali ions presumably provide transient coordination with the crown ether group in **6** and thereby reducing the disorder of the framework. The formulations of **5**−**8** were established by a combination of X-ray single crystal structure analysis, thermogravimetric analysis (TGA), and ^{1}H NMR studies.

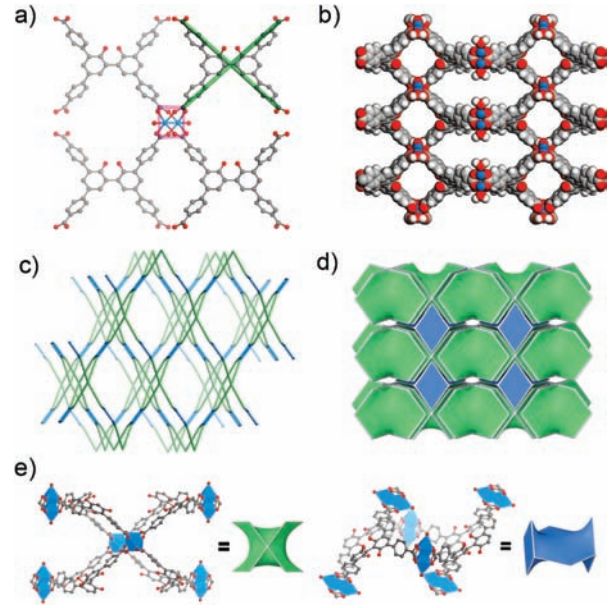

Figure 1. (a) Coordination geometry of $[Cu_2(O_2CR)_4]$ paddle-wheel in **5**: C, gray, Cu, blue, O, red, H atoms are omitted for clarity. Pink squares and green crosses represent $[Cu_2(O_2CR)_4]$ SBU and $\mathbf{L_1}$ ligand, respectively. (b) Space-filling model of **5** showing highly porous structure as viewed perpendicular to the (110) plane. (c) Schematic representation of the PtS topology of **5**. (d, e) Schematic representation of tiling for **5**.

Crystal Structure Analysis and Topological Studies. $[Cu_2(\mathbf{L_1})(H_2O)_2]\cdot 14DMF\cdot 10H_2O$ (**5**) crystallizes in the orthorhombic space group *Cccm* with a half Cu^{II} ion and a quarter of $\mathbf{L_1}$ in the asymmetric unit. Each Cu^{II} ion coordinates to four carboxylate groups from four $\mathbf{L_1}$ ligands and a water molecule in a square-pyramidal geometry. The four carboxylate groups bridge two Cu^{II} ions to form a $[Cu_2(O_2CR)_4]$ paddle-wheel secondary building units (SBU highlighted as pink square in Figure 1a). The $\mathbf{L_1}$ ligands which are simplified as green crosses have a dihedral angle of 55.76° and link the $[Cu_2(O_2CR)_4]$ SBUs to form a 3D open

(23) Eddaoudi, M.; Moler, D. B.; Li, H. L.; Chen, B. L.; Reineke, T. M.; O'Keeffe, M.; Yaghi, O. M. *Acc. Chem. Res.* **2001**, *34*, 319–330.
(24) Furukawa, H.; Kim, J.; Ockwig, N. W.; O'Keeffe, M.; Yaghi, O. M. *J. Am. Chem. Soc.* **2008**, *130*, 11650–11661.
(25) Wong-Foy, A. G.; Lebel, O.; Matzger, A. J. *J. Am. Chem. Soc.* **2007**, *129*, 15740–15741.
(26) Chui, S. S. Y.; Lo, S. M. F.; Charmant, J. P. H.; Orpen, A. G.; Williams, I. D. *Science* **1999**, *283*, 1148–1150.
(27) Ma, S. Q.; Zhou, H. C. *J. Am. Chem. Soc.* **2006**, *128*, 11734–11735.
(28) Lin, X.; Jia, J. H.; Zhao, X. B.; Thomas, K. M.; Blake, A. J.; Walker, G. S.; Champness, N. R.; Hubberstey, P.; Schröder, M. *Angew. Chem., Int. Ed.* **2006**, *45*, 7358–7364.
(29) Ma, L.; Lee, J. Y.; Li, J.; Lin, W. *Inorg. Chem.* **2008**, *47*, 3955–3957; we incorrectly identified the network topology of these compounds as the distorted PtS net in this paper.
(30) Reinhoudt, D. N.; de Jong, F.; van de Vondervoort, E. M. *Tetrahedron* **1981**, *37*, 1753–1762.
(31) Ngo, H. L.; Lin, W. *J. Am. Chem. Soc.* **2002**, *124*, 14298–14299.

framework with interconnecting channels (Figure 1b). Because both $[Cu_2(O_2CR)_4]$ SBUs and $\mathbf{L_1}$ ligands act as four-connected nodes, the framework of **5** is binodal and adopts the PtS network topology with the Schläfli symbols of $[4^2.8^4]$ (Figure 1c).[32−38] Tiling analysis showed that **5** contained two building blocks, tile $[8^4]$ and tile $[4^2.8^2]$ (as shown green and blue tiles in panels d and e of Figure 1).[39] The intrinsic symmetry for tiling is $P4_2/mmc$ with the transitivity [2132].

$[Cu_2(\mathbf{L_2})(H_2O)_2]\cdot 12DMF$ (**6**) crystallizes in the monoclinic space group $C2/c$ with four crystallographically unique Cu^{II} ions, one full $\mathbf{L_2}$ ligand, two half $\mathbf{L_2}$ ligands, and four coordinated water molecules in the asymmetric unit. **6** is isostructural to recently reported 3D MOFs $[Cu_2\mathbf{L_0}(H_2O)_2]\cdot 13DMF$ and $[Zn_2\mathbf{L_0}(H_2O)_2]\cdot 12DMF$ that were built from ligand $\mathbf{L_0}$.[29] The $\mathbf{L_2}$ ligands link the Cu^{II} ions to form three crystallographically independent $[Cu_2(O_2CR)_4]$ SBUs. Although the basic building units of **6** are essentially the same as those of **5**, the dihedral angles of $\mathbf{L_2}$ and the directions of the $[Cu_2(O_2CR)_4]$ SBUs in **6** are different from those in **5**. The dihedral angles for the central biphenyl rings of the $\mathbf{L_2}$ ligands are 89.55° (for $\mathbf{L_{2a}}$), 49.63° (for $\mathbf{L_{2b}}$), and 49.33° (for $\mathbf{L_{2c}}$), respectively. In **5**, there is only one unique $[Cu_2(O_2CR)_4]$ SBU, and all of them are parallel to each other in the crystal structure. Four nodes of $[Cu_2(O_2CR)_4]$ SBUs and four nodes of $\mathbf{L_1}$ ligands made up an octagon in **5**. In **6**, the paddle-wheels run along different directions, and as a result, three kinds of $[Cu_2(O_2CR)_4]$ SBUs and three kinds of $\mathbf{L_2}$ made up a hexagon (as shown in Figure 2a). Compound **6** is a thus 6-nodal net with the Schläfli symbol $[6^4.8^2]_3[6^6]$. All of the three $[Cu_2(O_2CR)_4]$ SBUs, as well as $\mathbf{L_{2b}}$ and $\mathbf{L_{2c}}$, exhibit $[6^4.8^2]$ point symbol whereas $\mathbf{L_{2a}}$ exhibits $[6^6]$ point symbol.

$[Zn_6(\mu_4\text{-}O)(\mathbf{L_1})_2(\mathbf{L_1}\text{-}H_2)]\cdot 35DMF\cdot 27H_2O$ (**7**) crystallizes in the orthorhombic space group $Pca2_1$ with six Zn^{II} ions, one μ_4-O atom, and three $\mathbf{L_1}$ ligands (one is fully deprotonated and the other two are monoprotonated) in the asymmetric unit. As shown in Figure 3a, two Zn^{II} ions adopt trigonal bipyramidal geometry whereas the other four Zn ions adopt distorted tetrahedral coordination geometry. All of the six Zn^{II} ions are involved in forming two kinds of SBUs: the $[Zn_4(\mu_4\text{-}O)(O_2CR)_7]$ cluster which serves as a 7-connected topological node and the $[Zn_2(O_2CR)_3(HO_2CR)_2]$ unit (a derivative of the $[Zn_2(O_2CR)_3]$ paddle wheel) that serves as a 5-connected topological node (Figure 3c). The dihedral angles for the three different ligands $\mathbf{L_1}$ ligands are 64.35°, 66.75°, and 76.67°, respectively. They behave as tetrahedral linkers that connect the $[Zn_4(\mu_4\text{-}O)(O_2CR)_7]$ units into a two-dimensional (2D) layer. The adjacent layers are further connected by the $[Zn_2(O_2CR)_3(HO_2CR)_2]$ units into a 3D open framework. The space-filling model of **7** shows a one-dimensional (1D) channel with a diameter of ~12.5 Å along the c axis (Figure 3b).

Compound **7** adopts a new topological type with five kinds of nodes. As shown in Figure 3c, the $[Zn_4(\mu_4\text{-}O)(O_2CR)_7]$

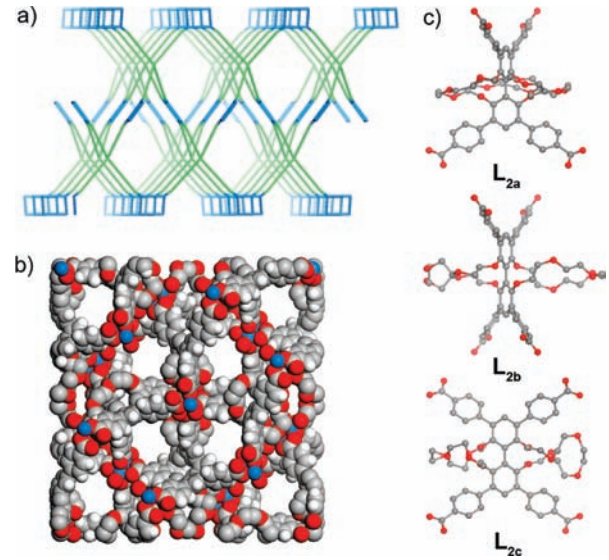

Figure 2. (a) Schematic representation of compound **6**. The blue square represents the $[Cu_2(O_2CR)_4]$ paddle wheel, the green tetrahedral skeleton represents $\mathbf{L_2}$. (b) The space-filling mode of **6**, showing the 1D channel along c axis. The color scheme is the same as Figure 1. (c) The representation of three crystallographically unique $\mathbf{L_2}$.

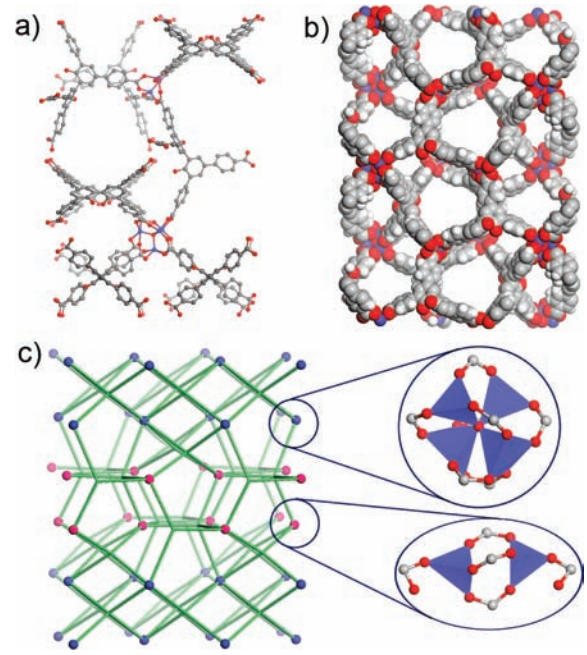

Figure 3. (a) Coordination geometry of $[Zn_2(O_2CR)_3(HO_2CR)_2]$ and $[Zn_4(\mu_4\text{-}O)(O_2CR)_7]$ in compound **7**: C, gray, Zn, violet, O, red, H atoms are omitted for clarity. (b) Space-filling model of **7** showing large open channels (with a diameter of ~12.5 Å) running along the c axis. (c) Schematic representation of the topology of **7**. The violet and magenta balls represent the $[Zn_4(\mu_4\text{-}O)(O_2CR)_7]$ and $[Zn_2(O_2CR)_3(HO_2CR)_2]$ SBUs respectively. The green crosses represent $\mathbf{L_1}$ ligands.

(32) Blatov, V. A.; Shevchenko, A. P.; Serezhkin, V. N. *Russ. J. Coord. Chem.* **1999**, *25*, 453M–465; http://www.topos.ssu.samara.ru.
(33) Chen, B. L.; Ockwig, N. W.; Fronczek, F. R.; Contreras, D. S.; Yaghi, O. M. *Inorg. Chem.* **2005**, *44*, 181–183.
(34) Friedrichs, O. D.; O'Keeffe, M.; Yaghi, O. M. *Solid State Sci.* **2003**, *5*, 73–78.
(35) Kim, J.; Chen, B. L.; Reineke, T. M.; Li, H. L.; Eddaoudi, M.; Moler, D. B.; O'Keeffe, M.; Yaghi, O. M. *J. Am. Chem. Soc.* **2001**, *123*, 8239–8247.
(36) Liu, B.; Li, B. L.; Li, Y. Z.; Chen, Y.; Bao, S. S.; Zheng, L. M. *Inorg. Chem.* **2007**, *46*, 8524–8532.
(37) Natarajan, R.; Savitha, G.; Dominiak, P.; Wozniak, K.; Moorthy, J. N. *Angew. Chem., Int. Ed.* **2005**, *44*, 2115–2119.
(38) Long, L. S.; Ren, Y. P.; Ma, L. H.; Jiang, Y. B.; Huang, R. B.; Zheng, L. S. *Inorg. Chem. Commun.* **2003**, *6*, 690–693.
(39) Delgado-Friedrichs, O.; O'Keeffe, M. *Acta Crystallogr.* **2003**, *A59*, 351–360; http://www.gavrog.org.

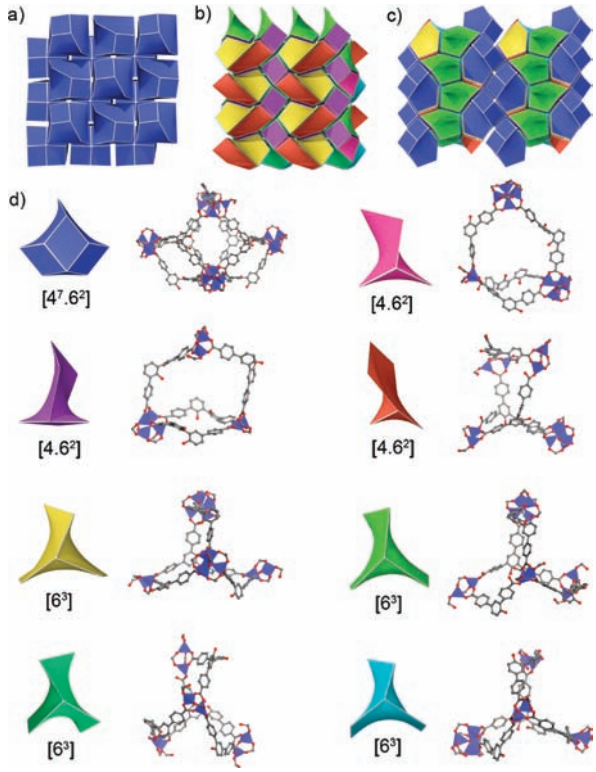

Figure 4. (a) View of the bilayer composed of blue tiles [$4^7.6^2$] down the *b* axis. (b) The representation of the layer made up of the rest seven kinds of tiles as viewed along the *b* axis. (c) The ABAB packing style in **7** as viewed along the *c* axis. (d) The list of eight tiles in **7**, including the shape of tiles, corresponding Schläfli symbols, and their structures.

and $[Zn_2(O_2CR)_3(HO_2CR)_2]$ SBUs act as distinct nodes, and the three crystallographically unique $\mathbf{L_1}$ also act as different nodes. The Schläfli symbol for each node is as follows: $[Zn_4(\mu_4\text{-}O)(O_2CR)_7]$, $[4^8.6^{10}.8^3]$; $[Zn_2(O_2CR)_3(HO_2CR)_2]$, $[4^2.6^8]$; $\mathbf{L_{1a}}$, $[4^5.6]$; $\mathbf{L_{1b}}$, $[4^4.6^2]$; and $\mathbf{L_{1c}}$, $[4.6^5]$. The network of **7** is made up of squares, pentagons, and heptagons with the stoichiometry of 3:1:1. Compound **7** can be considered to be made up of eight kinds of tiles (Figure 4d), with the transitivity [5(12)(15)8]. The blue tile, which is basket-shaped, is the major tile that self-assembles into a bilayer (Figure 4a). The rest seven tiles assemble to form a second layer (Figure 4b). These layers pack in the ABAB fashion to form a 3D framework (Figure 4c).

$[Zn_3Na_2(\mathbf{L_2})_2(DMF)_2]\cdot 7DMF\cdot 14H_2O$ (**8**) crystallizes in the monoclinic space group $P2_1/n$ with one and half Zn^{II} ions (Zn1 and Zn2), one $\mathbf{L_2}$, one Na^+ ion, and one DMF molecule in the asymmetric unit. The Zn1 ion adopts a tetrahedral geometry by coordinating to three bridging carboxylate groups and one monodentate carboxylate group of four different $\mathbf{L_2}$ ligands. The Zn2 ion is located on the *b* axis and adopts an octahedral geometry by coordinating to six bridging carboxylate groups. Two Zn1 and one Zn2 centers are connected by six carboxylate groups to form trinuclear SBUs which are linked by $\mathbf{L_2}$ ligands to form a 2D layer in the (010) plane. These 2D layers are further linked by the $\mathbf{L_2}$ ligands along the (101) plane to lead to a 3D framework. The Na^+ ions adopt distorted pentagonal bipyramid geometry by coordinating to the six oxygen atoms of the crown ether and one DMF molecule (Figure 5b).

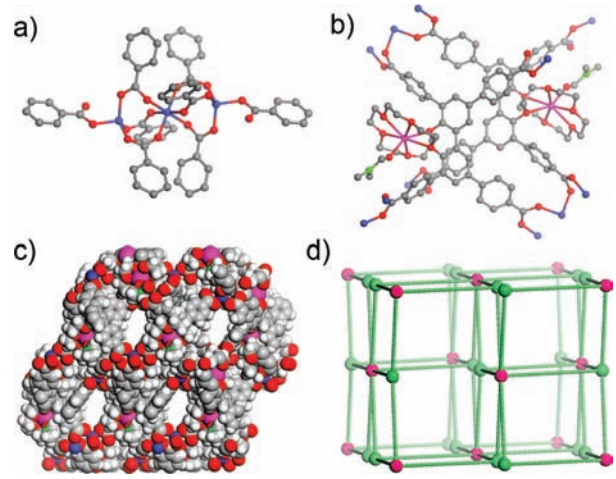

Figure 5. (a) Coordination geometry of $[Zn_3(O_2CR)_8]$ unit. H atoms were omitted for clarity. The color scheme is the same as Figure 3. (b) The representation of a pair of $\mathbf{L_2}$ with coordinated Zn^{II} ions, as well as the Na^+ ions and DMF molecules. Na, pink, N, blue. (c) Space-filling model of **8** showing small channels perpendicular to the plane (111). (d) Schematic representation of **8** showing the topology of $[4^{12}.6^{12}.8^4][4^6]_2$. The green ball represents the $\mathbf{L_2}$, while the pink ball represents the $[Zn_3(O_2CR)_8]$ unit.

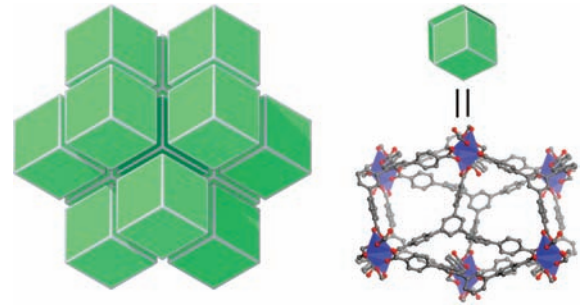

Figure 6. Left, representation of tiling for **8**. The dark green tile is surrounded by 12 light green tiles. Right, the structure of a single tile.

Since the $\mathbf{L_2}$ ligand is a 4-connected node and the $[Zn_3(O_2CR)_8]$ unit is a 8-connected node, compound **8** is a 2-nodal net and adopts the flu (fluorite) topology with the Schläfli symbol $[4^{12}.6^{12}.8^4][4^6]_2$ (Figure 5d).[40−42] The point symbol for $\mathbf{L_2}$ is $[4^6]$, whereas the point symbol for the $[Zn_3(O_2CR)_8]$ unit is $[4^{12}.6^{12}.8^4]$. The tile of **8** is cage-like, made up of six $[Zn_3(O_2CR)_8]$ unit nodes and eight $\mathbf{L_2}$ nodes (Figure 6). The point symbol for the tile is $[4^{12}]$, indicating that each tile is surrounded by 12 other tiles.

Gas Sorption Studies. The porosities and gas uptake behaviors of compound **5**−**8** were determined both experimentally and theoretically. X-ray structural analysis showed that **5** is highly porous with a framework density of 0.421 g/cm^3 and void volume of 80.8% as calculated by PLATON.[43] TGA analysis showed that **5** lost 57.12% weight because of solvent molecules, and the framework of **5** decomposed at temperatures above 250 °C. N_2 adsorption studies at 77 K gave a Langmuir surface area of 1217 m^2/g

(40) Zou, R. Q.; Zhong, R. Q.; Du, M.; Kiyobayashi, T.; Xu, Q. *Chem. Commun.* **2007**, 2467–2469.
(41) Chun, H.; Kim, D.; Dybtsev, D. N.; Kim, K. *Angew. Chem., Int. Ed.* **2004**, *43*, 971–974.
(42) Taylor K. M. L.; Athena J.; Lin, W. *Angew. Chem., Int. Ed.* **2008**, anie.200802911.
(43) Spek A. L., *PLATON, A Multipurpose Crystallographic Tool*; Utrecht University: Utrecht, The Netherlands, 2008.

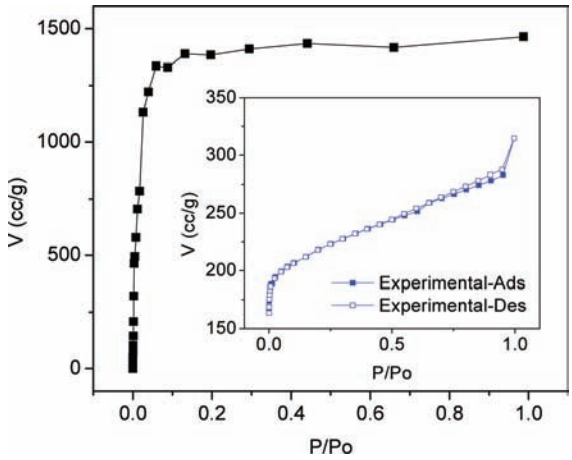

Figure 7. Calculated adsorption isotherms for **5**. The inset shows the experimental isotherms.

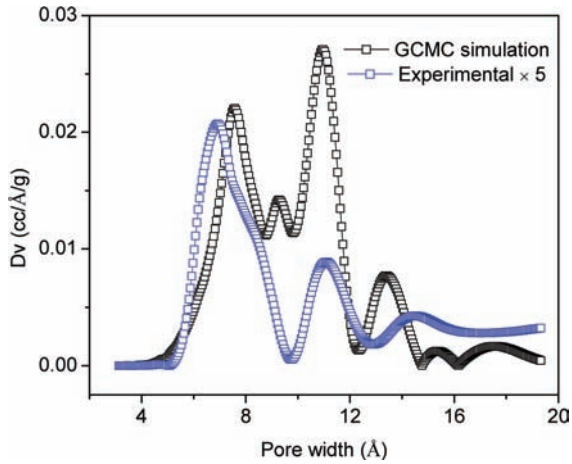

Figure 8. Pore size distribution of **5** calculated by the HK method.

for **5**. This Langmuir surface area is larger than that of the related Cu-$\mathbf{L_0}$ MOF (733 m^2/g),[29] consistent with the less steric demand of the dihydroxy group in $\mathbf{L_1}$ than the diethoxy group in $\mathbf{L_0}$. The experimental surface area of **5** is however much smaller than that given by the grand canonical Monte Carlo (GCMC) simulations. GCMC simulations gave a Langmuir surface area of 6043.88 m^2/g for **5**, with a majority of pores of about 7.6 and 11.0 Å in diameter as determined by the Horvath−Kawazoe (HK) method (Figures 7 and 8).[44] Powder X-ray diffraction (PXRD) patterns indicated that the framework structure of the evacuated sample of **5** has significantly distorted as the diffraction peaks (111) and (131) disappeared (Supporting Information, Figure S9). Such distortion of MOFs during evacuation is now well established[45−47] and can account for the discrepancy in the experimental and theoretical surface areas (as a result of the blockage of certain channels and cavities). Consistent with this, reduction in experimental pore sizes (from theoretical ones) is also evident in Figure 7. This hypothesis is further

(44) Horváth, G.; Kawazoe, K. *J. Chem. Eng. Jpn.* **1983**, *16*, 470–475.
(45) Barthelet, K.; Marrot, J.; Riou, D.; Férey, G. *Angew. Chem., Int. Ed.* **2002**, *41*, 281–284.
(46) Serre, C.; Millange, F.; Thouvenot, C.; Noguès, M.; Marsolier, G.; Louër, D.; Férey, G. *J. Am. Chem. Soc.* **2002**, *124*, 13519–13526.
(47) Férey, G.; Mellot-Draznieks, C.; Serre, C.; Millange, F. *Acc. Chem. Res.* **2005**, *38*, 217–225.

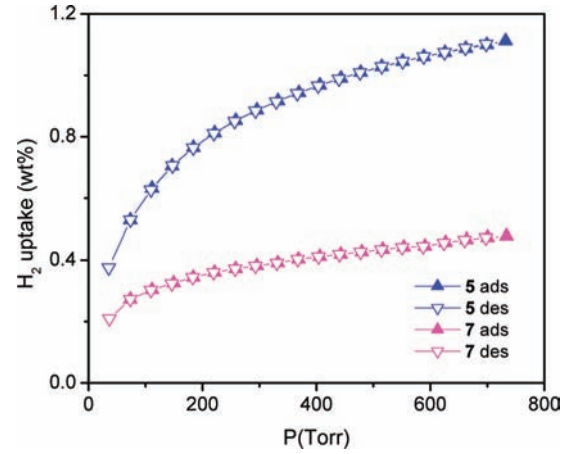

Figure 9. H_2 adsorption/desorption isotherm of compound **5** and **7**.

Table 1. Theoretical and Experimental Gas Uptake Results for **5**−**8**

sample	**5**	**6**	**7**	**8**
calcd density ($g\cdot cm^{-3}$)[a]	0.421	0.474	0.430	0.995
void volume %[a]	80.8	66.5	79.0	40.3
theoretical Langmuir SA ($m^2\cdot g^{-1}$)[b]	6043.88	4186.43	5711.62	1307.33
exp. Langmuir SA ($m^2\cdot g^{-1}$)	1217			
CO_2 uptake (wt %)	12.63	6.26	6.08	
H_2 uptake (wt %)	1.1		0.48	

[a] Calculated using PLATON;[43] [b] Calculated using Grand Canonical Monte Carlo (GCMC) simulations; SA stands for surface area.

supported by dye uptake experiments. **5** uptakes 43 wt % Rhodamine 6G and 78 wt % Brilliant Blue R-250, respectively (Supporting Information, Table S2). Dye-incorporated **5** exhibits the same powder X-ray diffraction patterns as the pristine solid (Supporting Information, Figure S16), suggesting stabilization of the framework (against distortion) after dye uptake. Although the framework of **5** exhibited significant distortion and a gas uptake significantly less than theoretical values, sorption experiments showed that **5** had a H_2 uptake of ∼1.1 wt % in 77 K (Figure 9). This hydrogen uptake capacity is slightly higher than that of the related Cu-$\mathbf{L_0}$ MOF (0.8 wt %).[29]

The framework distortion is even more severe for compounds **6**−**8**. Although GCMC simulations predicted large Langmuir surface areas (for N_2), experimental sorption studies showed no N_2 uptake for **6**−**8** (Table 1). Among them, only the evacuated sample of **7** has a modest H_2 uptake of 0.48% at 77 K. In the Cu family of MOFs, the gas uptake capacity ranks in the order of built from Cu-$\mathbf{L_1}$ > Cu-$\mathbf{L_0}$ > Cu-$\mathbf{L_2}$, consistent with the order of the increasing steric bulk among the dihydroxy, diethoxy, and the crown ether groups.[29]

Conclusions

A series of 3D Cu and Zn MOFs based on functionalized tetracarboxylate ligands have been prepared and their structures determined by single crystal X-ray diffraction studies. The three Cu MOFs based on the related ligands $\mathbf{L_0}$, $\mathbf{L_1}$, and $\mathbf{L_2}$ are built from similar paddle-wheel SUBs albeit with two slightly different network topologies. Compound **5** is highly porous with a Langmuir surface area of 1217 m^2/g and shows a H_2 uptake of 1.11 wt %. The three Zn compounds on the other hand have different SBUs and

adopt entirely different network topologies. These results further demonstrate the robustness of the paddle-wheel SBUs in Cu MOFs in maintaining the network connectivity and topology. The biphenol-derived tetracarboxylate ligands provide a highly tailorable system for building highly porous MOFs and for examining the dependence of MOF structures and topologies on ligand modifications.

Experimental Section

General Procedures and Materials. Certified ACS grade solvents (CH_2Cl_2, ethyl acetate, ethanol, hexane, and acetone) and anhydrous ethylene glycol diethyl ether (DME) were purchased from Fisher Scientific and used as received. Anhydrous THF was distilled over Na/benzophenone prior to use. 2,2′-Diethoxylbiphenyl-3,3′,5,5′-tetrakis(4-methylbenzoate) (**1**) and 3,3′,5,5′-tetrabromo-2,2′-biphenol (**2**) were synthesized according to the reported procedures.[29,48]

Synthesis of 2,2′-Biphenol-3,3′,5,5′-tetrakis(4-benzoic acid) (L_1-H_4). BBr_3 (3 mL, 19.7 mmol) was added to a solution of **1** (1.61 g, 2.07 mmol) in 50 mL of dichloromethane in a 250 mL round-bottom flask at 0 °C. The resulting solution was allowed to warm up to room temperature and stirred for an additional 8 h. The reaction mixture was then poured into 100 mL of ice/water. The resultant precipitate was extracted with ethyl acetate, and the organic layer was washed with water (3 × 200 mL), and then dried with anhydrous $MgSO_4$. After filtration, the solvent was removed in vacuo to yield 1.36 g of L_1-H_4 (98.5%) as a light pink solid. ^{1}H NMR (DMSO-d_6, 400 MHz): δ 7.702 (s, 2H), 7.706 (s, 2H), 7.832 (d, J_{HH} = 8.0 Hz, 4H), 7.896 (d, J_{HH} = 8.4 Hz 4H), 7.985 (d, J_{HH} = 8.4 Hz, 4H), 8.035 (d, J_{HH} = 8.4 Hz, 4H).

Synthesis of 3,3′,5,5′-Tetrabromo-2,2′-penta(ethylene glycol)-biphenyl (3). NaH (in 60% mineral oil, 0.41 g, 10.4 mmol) was slowly added to a solution of **2** (2 g, 4 mmol) in 130 mL of anhydrous THF in a 500 mL three-neck round-bottom flask at room temperature under Argon. The mixture was stirred for 10 min. Then a solution of penta(ethylene glycol) di-*p*-toluenesulfonate (2.60 g, 4.77 mmol) in 30 mL of anhydrous THF was added slowly. The mixture was stirred and heated to reflux for 2 days. After being cooled to room temperature, the mixture was poured into 300 mL of ethyl acetate. The organic layer was washed with water (3 × 200 mL) and dried with anhydrous $MgSO_4$. After filtration, the solvents were removed in vacuo. The resultant oil was washed with hexanes (3 × 20 mL) to yield **3** (1.31 g, 47%) as colorless crystals. ^{1}H NMR ($CDCl_3$, 400 MHz): δ 3.52−3.70 (m, 20H), 7.47 (d, $^3J_{HH}$ = 2.0 Hz, 2H), 7.67 (d, $^3J_{HH}$ = 2.0 Hz, 2H).

Synthesis of 2,2′-Penta(ethylene glycol)biphenyl-3,3′,5,5′-tetrakis(4-methylbenzoate) (4). Thirteen milliliters of DME was added to a mixture of **3** (0.81 g, 1.15 mmol) and 4-(methoxycarbonyl)-phenylboronic acid (1.66 g, 9.22 mmol) in a 100 mL pressure-tube. The solution was degassed with Argon for 30 min, then cesium fluoride (1.75 g, 11.5 mmol) and $Pd(PPh_3)_4$ (0.266 g, 0.23 mmol) were added. The resultant mixture was degassed for another 30 min, and then sealed and heated to 100 °C for 2 days. After being cooled to room temperature, the mixture was poured into 300 mL of ethyl acetate. The organic layer was washed with water (3 × 200 mL) and dried with anhydrous $MgSO_4$. After filtration, the solvents were removed in vacuo. The resulting material was purified by flash column chromatography using silica gel and 11% (v/v) acetone in ethyl acetate as the eluent to yield **4** as a white solid (0.81 g, 75.8%). ^{1}H NMR ($CDCl_3$, 400 MHz): δ 3.290−3.764 (m, 20H), 3.964 (s, 6H), 3.983 (s, 6H), 7.673 (s, 2H), 7.740 (d, J_{HH} = 8.4 Hz, 4H), 7.799 (s, 2H), 7.833 (d, J_{HH} = 8.4 Hz 4H), 8.130 (d, J_{HH} = 8.4 Hz, 4H), 8.161 (d, J_{HH} = 8.4 Hz, 4H).

Synthesis of 2,2′-Penta(ethylene glycol)biphenyl-3,3′,5,5′-tetrakis(4-benzoic acid) (L_2-H_4). To a solution of **4** (0.81 g, 0.87 mmol) in 10 mL of THF was added 50 mL of H_2O and NaOH aqueous solution (6M, 15 mL). The mixture was heated to reflux for overnight. After being cooled down to room temperature, aqueous HCl solution (10 wt %, 30 mL) was added to the reaction mixture, which was stirred for an additional 2 h. The resultant precipitate was filtered and washed with water (3 × 50 mL). After being dried in vacuo, 0.71 g of L_2-H_4 was obtained as a white solid (93.4%). ^{1}H NMR (DMSO-d_6, 400 MHz): δ 3.230−3.547 (m, 20H), 7.814 (s, 2H), 7.859 (s, 2H), 7.900 (d, J_{HH} = 8.4 Hz, 4H), 7.956 (d, J_{HH} = 8.4 Hz, 4H), 8.015 (d, J_{HH} = 8.4 Hz, 4H), 8.059 (d, J_{HH} = 8.4 Hz, 4H).

Synthesis of $[Cu_2(L_1)(H_2O)_2]\cdot 14DMF\cdot 10H_2O$ (5). Slow diffusion of toluene into a mixture of $Cu(NO_3)_2\cdot 6H_2O$ (9.64 mg, 0.04 mmol), L_1-H_4 (13.3 mg, 0.02 mmol) and *trans*-diaminocyclohexane (3.42 μL, 0.03 mmol) in DMF/H_2O (1 mL/0.4 mL) at 60 °C for overnight. Green column-shaped single crystals were filtered and dried with filter paper to adsorb mother liquid on the crystal surface. Yield: 26.26 mg (66% based on L_1). IR (cm^{-1}): 1657vs, 1651vs, 1607s, 1556w, 1499w, 1435w, 1383vs, 1252m, 1178w, 1092s, 1063w, 1016w, 893w, 862w, 785m, 750w, 727m, 712m, 658s.

Synthesis of $[Cu_2(L_2)(H_2O)_2]\cdot 12DMF$ (6). A mixture of $Cu(NO_3)_2\cdot 3H_2O$ (3.61 mg, 0.015 mmol), L_2-H_4 (2.6 mg, 0.003 mmol), HCl (2 μL, 0.01 mmol), DMF (0.33 mL), and H_2O (0.13 mL) was heated to 80 °C overnight. Blue block-shaped single crystals were filtered and dried with filter paper to adsorb mother liquid on the crystal surface (4.98 mg, 87%, based on L_2). IR (cm^{-1}): 1661vs, 1651vs, 1614s, 1558w, 1498w, 1437w, 1385vs, 1252m, 1180w, 1094s, 1063w, 1016w, 947w, 862w, 843m, 785m, 750w, 727w, 714m, 660s.

Synthesis of $[Zn_6(\mu_4\text{-}O)(L_1)_2(L_1\text{-}H_2)]\cdot 35DMF\cdot 27H_2O$ (7). Slow diffusion of toluene/ethanol (1:1, v/v) into a mixture of $Zn(NO_3)_2\cdot 6H_2O$ (2.98 mg, 0.01 mmol), L_1-H_4 (3.3 mg, 0.005 mmol), pyridine (1 μL, 0.0125 mmol), DMF (1 mL), H_2O (0.2 mL) at 60 °C for a week. Colorless clusters of crystals were filtered and dried with filter paper to adsorb mother liquid on the crystal surface (2.33 mg, 25.6%, based on L_1). IR (cm^{-1}): 1699m, 1593m, 1537m, 1510m, 1393s, 1358s, 1221m, 1182w, 1088w, 1063w, 1016w, 893w, 860w, 785m, 752w, 710m, 665w.

Synthesis of $[Zn_3Na_2(L_2)_2(DMF)_2]\cdot 7DMF\cdot 14H_2O$ (8). Slow diffusion of toluene into a mixture of $Zn(NO_3)_2\cdot 6H_2O$ (2.98 mg, 0.01 mmol), L_2-H_4 (4.34 mg, 0.005 mmol), HCl (20 μL, 0.02 mmol), and DMF (1 mL) at 60 °C. White polycrystalline materials formed after 2 weeks, which transformed to colorless block-shaped single crystals in a month. The crystals were harvested and dried with filter paper to adsorb mother liquid on the crystal surface (4.22 mg, 87%, based on L_2). IR (cm^{-1}): 1661s, 1651s, 1603m, 1553w, 1504w, 1435w, 1362s, 1248w, 1219w, 1190w, 1095m, 1063w, 1015w, 947w, 866w, 787m, 727m, 714m, 660m.

X-ray Studies. Crystallographic measurements for **5**−**8** were made on the Bruker SMART Apex II CCD-based X-ray diffractometer equipped with X-ray tube (Cu-target for **5**, **6**, and **8**, λ = 1.54178 Å; Mo-target for **7**, λ = 0.71073 Å) at 293 K for **5** and **7**, 223 K for **6** and **8**, respectively. The frames were integrated with the Bruker SAINT build in APEX II software package using a narrow-frame integration algorithm, which also corrects for the Lorentz and polarization effects. Absorption corrections were applied by using multiscan program SADABS. The structures were

(48) GómezLor, B.; Echavarren, A. M.; Santos, A. *Tetrahedron Lett.* **1997**, *38*, 5347–5350.

Table 2. Crystal Data and Structure Refinement Details for **5**−**8**

complex	**5**	**6**	**7**	**8**
crystal system	orthorhombic	monoclinic	orthorhombic	monoclinic
space group	*Cccm*	*C*2/*c*	$Pca2_1$	$P2_1/n$
a (Å)	15.9568(15)	41.5112(18)	28.833(5)	17.075(11)
b (Å)	29.329(2)	41.4556(18)	41.687(7)	20.519(13)
c (Å)	28.657(2)	31.1677(15)	30.561(5)	20.205(13)
α (deg)	90	90	90	90
β (deg)	90	109.408(3)	90	90.12(3)
γ (deg)	90	90	90	90
V (Å^3)	13411.3(19)	50588(4)	36733(10)	7079(8)
Z	8	2	4	2
D (g·cm^{-3})	0.423	0.526	0.432	0.995
μ/mm^{-1}	0.561	0.642	0.409	1.136
data/restraints/parameter	3486/96/136	25951/74/852	35821/1737/1213	3641/412/439
θ range/deg	3.01 to 49.98	1.55 to 50.46	1.09 to 20.85	3.07 to 40.00
obs reflns	1997	12526	10019	2316
R_1 ($I > 2\theta$ (I)) (squeeze)	0.0571	0.1086	0.0652	0.1070
*wR*2 (all data)	0.1708	0.3122	0.1740	0.3064

solved by direct method, and non-hydrogen atoms were refined anisotropically by least-squares on F^2 using the SHELX-XL program, except the disordered crown ether groups. The hydrogen atoms of aromatic phenyl rings were generated geometrically (C−H, 0.96 Å). The SQUEEZE subroutine of the PLATON software suite was applied to remove the scattering from the highly disordered solvent molecules. The resulting new HKL4 files were used to further refine the structures. Because of the relatively weak diffraction and low resolution (∼1Å), which is the result of the highly porous framework, the reflections at high resolution (<1Å) are ignored. Restraint (SIMU, DELU) on displacement parameters are applied. All the phenyl rings are constrained to ideal hexagons. Crystal data as well as the data collection and refinements details are summarized in Table 2.

The topology and tiling analysis for compound **5**−**8** are studied by using TOPOs 4.0.[32] The figures of tiling are generated in the software 3dt 0.3.2.[39]

Gas Sorption Studies. Using the Universal Force Field in conjunction with grand canonical Monte Carlo (GCMC) simulation, we calculated nitrogen adsorption isotherms, at 77 K, for the 3D MOFs **5**−**8**. The fugacity was set from 10^{-5} to 100 kPa. The experimental gas sorption measurements were carried on a Quantachrome Autosorb-1 instrument. While the Langmuir surface areas are calculated from both the simulated and experimental isotherm, the pore size distributions are analyzed by HK method.[44]

Acknowledgment. W.L. acknowledges NSF-DMR for financial support. S.W. thanks the China Scholarship Council for a State Scholarship Fund.

Supporting Information Available: Crystallographic information files (CIF) for complexes **5**−**8**, TGA results, X-ray powder diffraction patterns, and gas uptake experimental procedures. This material is available free of charge via the Internet at http://pubs.acs.org.

IC801631W